PAPER

Sensitive colorimetric detection of ochratoxin A by a dual-functional Au/Fe₃O₄ nanohybrid-based aptasensor

Rong Huang, Lu Lu Xiong, Hui Hui Chai, Jing Jing Fu, Zhisong Lu [ID]* and Ling Yu [ID]*

A novel colorimetric aptasensor based on a Au/Fe₃O₄ nanohybrid was developed to detect ochratoxin A (OTA). The aptasensor is composed of a free OTA aptamer, a Au/Fe₃O₄ nanohybrid coated with biotinylated complementary DNA of the OTA aptamer (biotin-cDNA-Au/Fe₃O₄), and free alkaline-phosphatase-labeled streptavidin (SA-ALP). The Au/Fe₃O₄ nanohybrid not only immobilizes biotin-cDNA but also magnetically separates SA-ALP from the sample solution. One part of the OTA aptamer sequence hybridizes with biotin-cDNA immobilized on Au/Fe₃O₄, and the left part of the OTA aptamer sequence covers the biotin and blocks the specific interaction between biotin and SA-ALP. OTA can interrupt the interaction of OTA aptamer binding to biotin-cDNA-Au/Fe₃O₄ and can inhibit the shielding effect of the OTA aptamer on biotin. The amount of SA-ALP that can be captured by biotin-cDNA-Au/Fe₃O₄ thus increases with increasing OTA concentration. Through a simple magnetic separation, the collected SA-ALP-linked Au/Fe₃O₄ can produce a yellow-colored solution in the presence of *p*-nitrophenyl phosphate (*p*-NPP). This colorimetric aptasensor can detect OTA as low as 1.15 ng mL⁻¹ with high specificity.

Introduction

Ochratoxin A (OTA) is a ubiquitous mycotoxin and is produced by various species of *Aspergillus* and *Penicillium*. It can potentially contaminate cereals (wheat, corn, and barley) and wines.[1,2] Several studies have suggested that OTA has nephrotoxicity, hepatotoxicity, neurotoxicity, and immunotoxicity.[2,3] Gastrointestinal damage, lymphatic lesions, bone marrow toxicity, and digestive disorders have also been reported in animal studies.[4,5] OTA has been classified as a group 2B "possibly carcinogenic to humans" by the International Agency for Research on Cancer (IARC).[2] The European Commission has established regulatory limits for raw cereal grains (5 μg kg⁻¹), roasted coffee (5 μg kg⁻¹), grape juice and all types of wine (2 μg kg⁻¹), and dried fruits (10 μg kg⁻¹).[6,7] Therefore, it is crucial to have a suitable analysis technique for high sensitivity detection of OTA.

Conventional methods for OTA quantification are based on instruments such as high-performance liquid chromatography[8,9] (HPLC) connected to fluorescence[10] or tandem mass spectrometry.[11–13] However, the high cost and sophisticated equipment as well as the time and labor costs and need for trained operators have hindered their applications.[14,15] Thus,

Key Laboratory of Luminescent and Real-Time Analytical Chemistry, Ministry of Education, Institute for Clean Energy and Advanced Materials, School of Materials and Energy, Southwest University, Chongqing 400715, PR China. E-mail: lingyu12@swu.edu.cn; zslu@swu.edu.cn

low-cost, convenient, and user-friendly detection of OTA is highly desired.

Colorimetric analysis can be easily monitored with the naked eye. It is affordable and simple, especially for field analysis.[16,17] Aptamers are single-stranded oligonucleotides that can specifically bind to their target molecules with high binding affinity.[18–22] Nanoparticle (NP)-based bioanalysis has attracted tremendous attention due to its high specific surface area and size-dependent optical properties.[3,23–26] Previously, OTA has been detected with gold nanoparticles (AuNPs) and nanographite homogenous reaction systems.[27] In those studies, the samples were directly mixed with the sensing solution,[28,29] and the change in fluorescent signal or color can be read without further separation. In one example of colorimetric detection, Xiao reported a OTA detection aptasensor based on analyte-induced assembling of oriented AuNP dimers.[28] Asymmetric functionalization of Au by DNA prevented the formation of large Au aggregates, and a Y-shaped DNA duplex was utilized to minimize the inter-particle distance. However, the sample solution properties such as color (wine, peanut oil, *etc.*) would interfere with the signal readout—especially for a colorimetric detection scheme. Thus, the isolation or separation of trace amounts of target from complex samples as well as their specific detection would potentially minimize the interference induced by the sample color.

Centrifugation is common in NP separation, but Fe₃O₄ NPs can be separated under a magnetic field. However, immobilization of probes on Fe₃O₄ NPs was compromised because they

often lack functional groups for covalent conjugation; thus, functionalization of Fe_3O_4 NPs was often required. For instance, a silicon oxide layer was coated on Fe_3O_4 NPs. Then, a SiO_2 layer was built with 3-aminopropyltrimethoxysilane (APTES) to introduce NH_2 groups for covalent probe immobilization.[30] The interaction between amino and aldehyde groups allows researchers to link DNA to Fe_3O_4. However, this process requires multi-step reactions and cross-linking reagents. For instance, Wang *et al.* reported a colorimetric aptasensor of OTA using Au@Fe_3O_4 and glass beads with a sophisticated reaction. The amino group was first coupled with the exposed hydroxyl groups on the Au@Fe_3O_4 surface to yield an amino-terminated self-assembled monolayer. The distal amino groups on Au@Fe_3O_4 surfaces were then reacted with aldehyde groups to immobilize amino-modified cDNA. While, additional glass beads were used to immobilize the aptamers.[31]

The intrinsic interaction between thiol group and gold has motivated researchers to immobilize DNA on Au. Here, we propose an Au/Fe_3O_4 aptasensor to achieve fast separation and colorimetric detection of OTA. The Au/Fe_3O_4 nanohybrids offer magnetic separation and immobilize probes for OTA detection. The 3′-end and 5′-end of the OTA aptamer recombinant cDNA fragment are tagged with a biotin and a thiol group, respectively (biotin-cDNA$_{OTA}$-SH). The mechanism is that binding of OTA aptamer with biotin-cDNA$_{OTA}$ to shield the biotin and thus inhibit the interaction of biotin with streptavidin-alkaline phosphatase (SA-ALP). The binding of OTA with OTA aptamer will set free the cDNA-biotin, leading to an increase in SA-ALP capture. The ALP can specifically hydrolyze its substrate *p*-nitrophenyl phosphate (*p*-NPP) to *p*-nitrophenol, which is a yellow complex with an intense absorption band at ~405 nm. This colorimetric change is proportional to the OTA concentration. We first optimized the amount of biotin-cDNA$_{OTA}$-SH and OTA aptamer in the sensing system and then evaluated the working range and detection limit. Next, the potential of the proposed Au/Fe_3O_4-based aptasensors was demonstrated by assaying OTA in peanut, corn, and wine samples. The results were compared with commercial OTA ELISA kit to prove its potential in real sample testing.

Materials and methods

Chemical and reagents

The sequence of OTA aptamer was 5′-GAT CGG GTG TGG GTGGCG TAA AGG GAG CAT CGG ACA-3′[32] and the sequence of its partially complementary oligonucleotide was 5′-SH-TGTCCG ATG CTC CCT TTA-C6-biotin-3′ (biotin-cDNA-SH). Both of them were chemically synthesized and purified by Sangon Biotech Co. Ltd. (Shanghai, China). $FeCl_3 \cdot 6H_2O$, $FeCl_2 \cdot 4H_2O$ were ordered from Aladdin Chemistry Co. Ltd. (Shanghai, China). Ammonio solution was purchased from Sinopharm Chemical Reagent Co., Ltd. $HAuCl_4$ was purchased from Rhawn reagent (Shanghai, China), and trisodium citrate dihydrate was purchased from Kelong Chemical Reagent Factory (Chengdu, China). OTA was obtained from Cayman chemical (USA). Aflatoxin (AFB1), fumonisin B1 (FB1), and deoxynivalenol (DON) from Fermentek Ltd. (Israel). Phosphate buffered solution (PBS)

was purchased from Beijing Dingguo Changsheng Biotechnology Co., Ltd. (Beijing, China). Tris was purchased from Genview (USA), and *p*-NPP, SA-ALP were purchased from Sigma-Aldrich (USA). A commercial OTA sandwich ELISA kit was purchased from Shanghai Youlong Biotech Co., Ltd. (Shanghai, China).

Synthesis of Au/Fe_3O_4 nanohybrid

First, Fe_3O_4 NPs were synthesized with a coprecipitation method.[33] In brief, $FeCl_3 \cdot 6H_2O$ (3.244 g) and $FeCl_2 \cdot 4H_2O$ (1.192 g) were dissolved in water (80 mL), and then 15 mL ammonia solution (28%, w/v%) was added. The solution was left undisturbed for 10 min at room temperature. The mixture was incubated at 90 °C with constant mechanical stirring under nitrogen gas protection. After 30 min, the Fe_3O_4 NPs were isolated with a permanent magnetic and washed several times with DI water. Finally, the Fe_3O_4 NPs were dried at 45 °C under vacuum for 24 h. To synthesize Au/Fe_3O_4 nanohybrid, the $HAuCl_4$ solution (0.04%, 50 mL) was boiled with constant stirring. Then, 500 μL Fe_3O_4 NPs and 1 mL 5% sodium citrate solution were added. The color of the solution changed from brown to purple and finally turned red. Stirring was continued for 10 min after the color change stopped. The heating source was removed, and stirring was continued for 15 min at room temperature. After the reaction, the Au/Fe_3O_4 hybrids were harvested by magnetic separation. The pellet was then washed several times and re-dispersed in DI water and stored at 4 °C.

Characterization of Au/Fe_3O_4 nanohybrid

The X-ray diffraction (XRD) patterns of the synthesized Au/Fe_3O_4 nanohybrid were obtained using an XRD-7000 (Shimadzu, Japan) with Cu-Kα source radiation. The morphology of the Au/Fe_3O_4 was investigated by a transmission electron microscopy (TEM, Tecnai G2 F20, FEI, USA). The chemical status of the Au/Fe_3O_4 was characterized by X-ray photoelectron spectroscopy (XPS, Escalab 250xi, Thermo Fisher, USA). The size of Fe_3O_4 NP and Au/Fe_3O_4 nanohybrids was measured using a Malvern Zetasizer Nano ZS 90 (Malvern, UK). The magnetic properties of Fe_3O_4 NP and Au/Fe_3O_4 nanohybrids were characterized by a vibrating sample magnetometer (VSM, MPMS Squid-VSM, USA).

Construction of biotin-cDNA$_{OTA}$-Au/Fe_3O_4 NP-based OTA aptasensor for colorimetric detection of OTA

A vial of received biotin-cDNA$_{OTA}$-SH was dissolved with 0.01 M PBS to obtain the stock solution with a concentration of 100 μM. Next, 5 μL 100 μM biotin-cDNA$_{OTA}$-SH was mixed with Au/Fe_3O_4, and then incubated at 37 °C for 40 h. To remove the unconjugated oligonucleotides, biotin-cDNA$_{OTA}$-Au/Fe_3O_4 NPs conjugates were collected and washed three times with magnetic separation. The collected biotin-cDNA$_{OTA}$-Au/Fe_3O_4 NPs were used for the OTA aptasensors construction.

OTA was dissolved in methanol for a stock solution with a concentration of 2 mg mL^{-1}. PBS was then used as a solvent to prepare working solutions with various concentrations of OTA as indicated. Different concentrations of OTA solution were

mixed with excess aptamer (20 μM) and allowed to react at room temperature for 30 min. The biotin-cDNA$_{OTA}$-Au/Fe$_3$O$_4$ was heated to 45 °C for 30 min and then incubated with the OTA-aptamer mixture overnight at room temperature. Then 50 μL of 1.5 mg L^{-1} SA-ALP (dissolved in pH = 8.0, 0.01 M Tris–HCl buffer) was added to 50 μL of the reaction solution and incubated at 37 °C for 1 h. The nano-hybrids pellet was washed three times with Tris–HCl buffer *via* magnetic separation. Next, 50 μL *p*-NPP was added to the collected Au/Fe$_3$O$_4$ pellet and incubated for 1 h at 37 °C. Finally, the absorption spectrum was recorded after adding 100 μL of 3 M NaOH stop solution. OTA at 100 pg mL^{-1}, 1 ng mL^{-1}, 10 ng mL^{-1}, 100 ng mL^{-1}, 1 μg mL^{-1}, 10 μg mL^{-1}, and 100 μg mL^{-1} were tested. The OTA induced colorimetric change was characterized by calculating the change of absorbance at 405 nm as follows:

$$\Delta A = |(A_{OTA} - A_0)/A_0|,$$

where A_0 is the absorbance of substrate without OTA, and A_{OTA} is the absorbance of substrate with different concentrations of OTA.

Specificity of biotin-cDNA$_{OTA}$-Au/Fe$_3$O$_4$ NP-based OTA aptasensor

To evaluate the specificity of the as proposed OTA aptasensor, other mycotoxicins [AFB1 (100 ng mL^{-1}), FB1 (100 ng mL^{-1}), and DON (100 ng mL^{-1})] were measured following the procedure as detailed above.

In addition, peanut, corn extracts and wine were used to test the feasibility of the biotin-cDNA$_{OTA}$-Au/Fe$_3$O$_4$ NP-based on aptasensor as described previously. The extracts were obtained following a protocol from literature.[34] Then the extracts were passed through a 0.22 μm syringe filter, and the OTA was added into the peanut, corn and wine samples at a final concentration of 5, 10, and 20 ng mL^{-1} and measured by the biotin-cDNA$_{OTA}$-Au/Fe$_3$O$_4$ NP-based OTA aptasensor. At the same time, the samples were measured by the commercial ELISA kit according to product instructions to validate the results obtained from as prepared OTA aptasensor.

Statistics analysis

All experiments were repeated three times and in triplicate. Data are expressed as the mean ± standard deviation. Experiment results were analyzed with the Student's *t*-test using Origin Statistic software (OriginLab, USA). *P* values less than 0.05 were considered statistically significant.

Results and discussion

Working principle of biotin-cDNA$_{OTA}$-Au/Fe$_3$O$_4$ NP-based OTA aptasensor
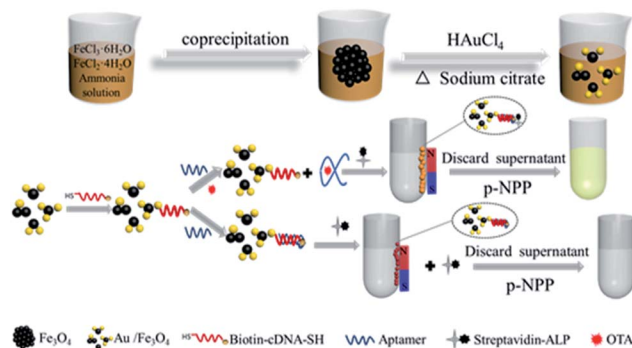
The colorimetric detection of OTA based on Au/Fe$_3$O$_4$ NPs is illustrated in Scheme 1. Here, the OTA aptamer works as a shielding cap to modulate the interaction between SA and biotin. Specifically, in the absence of OTA, the aptamer binds to its partially cDNA probes that immobilized on Au/Fe$_3$O$_4$, while

the unpaired bases at the 5′-end of OTA aptamer cover the biotin molecule at the end of cDNA. This inhibits the biotin–streptavidin interaction and further blocks the conjunction of ALP. After magnetic separation, there are fewer ALP captured by biotin-cDNA probes resulting in a lighter yellow color when the *p*-NPP substrate is added. However, in the presence of OTA, the hybridized aptamer is detached from its complementary DNA because the aptamer prefers to bind with OTA. The biotin molecule at the end of the complementary DNA is uncovered leading to high accessibility for the SA-ALP in solution. The increased ALP leads to a stronger *p*-NPP color change. The NPs could be removed magnetically, and the absorbance of the supernatant reflects the OTA concentration.
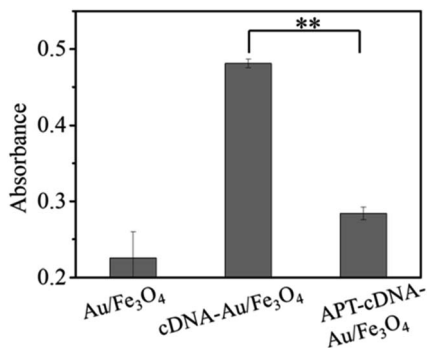
First, the shielding effect of OTA aptamer on biotin–streptavidin interaction was studied. Fig. 1 shows that less *p*-NPP is catalyzed with lower 405 nm absorbance when directly adding SA-ALP to the Au/Fe$_3$O$_4$ hybrids. However, adding SA-ALP into biotin-cDNA$_{OTA}$-Au/Fe$_3$O$_4$ hybrids can increase the amount of SA-ALP immobilization and thus significantly increase the absorbance to 0.48 ± 0.006. Adding OTA aptamer to the biotin-cDNA$_{OTA}$-Au/Fe$_3$O$_4$ hybrides can reduce the absorbance to 0.28 ± 0.008 because the unpaired base at the 5′ end blocks the biotin molecule at the end of the cDNA and reduces the binding of SA-ALP.

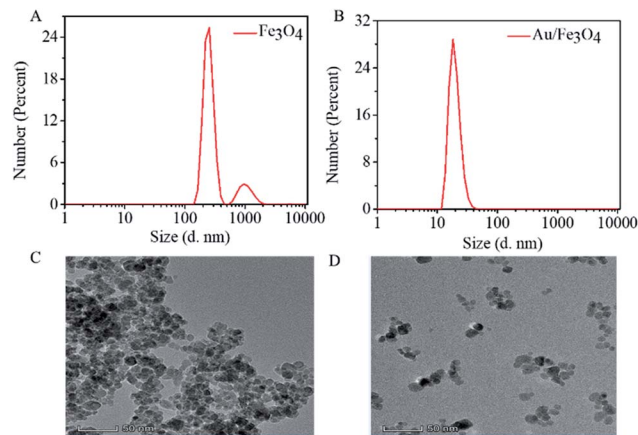### Characterization of the Au/Fe$_3$O$_4$ hybrids

Magnetic properties of Fe$_3$O$_4$ and nanohybrid were demonstrated by VSM. The magnetization loops are shown in Fig. 2A. Low coercivity of remanence existing at 300 K indicated the superparamagnetic behaviors of the two nanoparticles. The saturation magnetization value of Fe$_3$O$_4$ was calculated to be 84.4 emu g^{-1}. The value decreased to 67.9 emu g^{-1} after reacting with gold. The color of the Fe$_3$O$_4$ was black, and that of Au/Fe$_3$O$_4$ nanohybrid was dark red (inset of Fig. 2A). Though the magnetic strength of Au/Fe$_3$O$_4$ decreased, it can be easily attracted by an external magnetic field, which shows its significant magnetic separation capacity. The UV-visible absorption spectra of Fe$_3$O$_4$ and nanohybrid were measured because the Au was incorporated to provide a base for probe immobilization *via* the thiol group and Au interactions. A new peak at 532 nm was
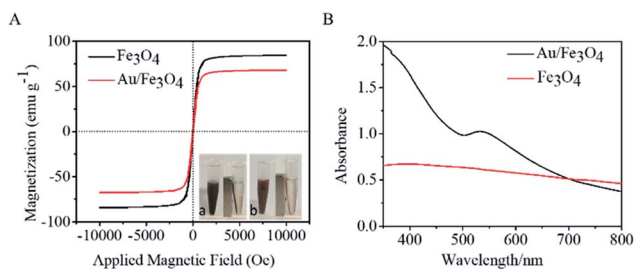

Scheme 1 Schematic illustration of the biotin-cDNA$_{OTA}$-Au/Fe$_3$O$_4$ NP-based OTA aptasensor for colorimetric detection of OTA.

Fig. 1 Shielding effect of OTA aptamer on the biotin–streptavidin interaction. Au/Fe_3O_4: Au/Fe_3O_4 nanohybrids. $cDNA-Au/Fe_3O_4$: Biotin-$cDNA_{OTA}$-Au/Fe_3O_4 hybrids. APT-$cDNA$-Au/Fe_3O_4: Biotin-$cDNA_{OTA}$-Au/Fe_3O_4 nanohybrids react with OTA aptamer. ** indicates $p < 0.01$.

Fig. 2 Characterization of $AuNP/Fe_3O$ nanohybrid. (A) Magnetic hysteresis loops of pure Fe_3O_4 and Au/Fe_3O_4 NP. Inset: the magnetic separation of Fe_3O_4 NP (a) and Au/Fe_3O_4 nanohybrid (b); (B) UV-vis spectra of Fe_3O_4 NP and Au/Fe_3O_4 nanohybrid.

observed for Au/Fe_3O_4 (Fig. 2B) *versus* pure Fe_3O_4 NPs indicating the existence of Au in the hybrids.
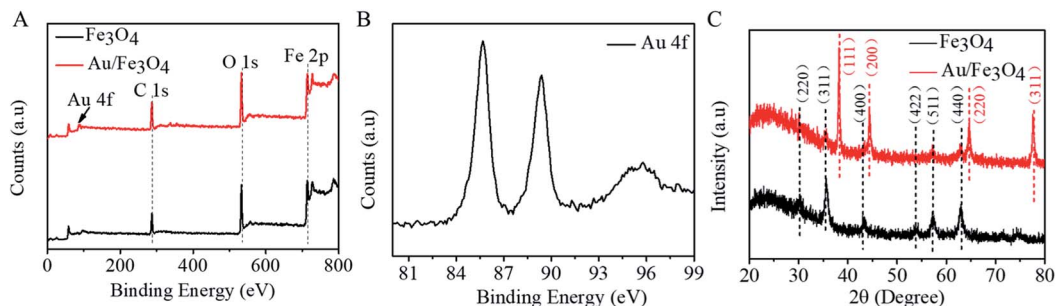
The chemical composition of Au/Fe_3O_4 nanohybrid was further ascertained by XPS measurements. The peaks of C, O, Au, and Fe elements were successfully observed in Au/Fe_3O_4 nanohybrid. In contrast, the peak of Au was not found in the XPS image of Fe_3O_4 (Fig. 3A). In the Au 4f core-level photo-electron spectrum of the Au/Fe_3O_4 nanohybrid (Fig. 3B), the peaks at 85.1 and 89.2 eV can be attributed to the Au $4d_{7/2}$ and Au $4f_{5/2}$ of metallic Au, respectively.[35] XRD characterization

Fig. 4 Dispersion of $AuNP/Fe_3O_4$ nanohybrid. Hydration particle size of (A) Fe_3O_4 and (B) Au/Fe_3O_4; TEM image of (C) Fe_3O_4 and (D) Au/Fe_3O_4.

showed typical XRD diffraction peaks at 2θ values of 30.1°, 35.5°, 43.1°, 53.5°, 57.0°, and 62.6° indexed to (220), (311), (400), (422), (511), and (440) planes of a cubic structure of Fe_3O_4 (JCPDS no. 19-0629), respectively. These were observed from both the pure Fe_3O_4 NP and Au/Fe_3O_4 nanohybrids (Fig. 3C). Four additional peaks centered at 38.1°, 44.3°, 64.5°, and 77.6° appeared for the Au/Fe_3O_4 nanohybrid, which can be attributed to the (111), (200), (220), and (311) planes for the face-centered-cubic gold (JCPDS no. 04-0784), respectively.[31]

The size of Fe_3O_4 NP and Au/Fe_3O_4 nanohybrids was characterized by dynamic light scattering. The hydrated particle size of Fe_3O_4 is more than 100 nm, and even several hundred nm, suggesting aggregation of Fe_3O_4 NP (Fig. 4A). However, the Au/Fe_3O_4 nanohybrid scatters with hydrated particle size of tens of nanometers (Fig. 4B). The TEM images shown in Fig. 4C and D further prove that incorporation of Au onto Fe_3O_4 NP can reduce the aggregation of the magnetic nanoparticle. The uniform dispersion of the Au/Fe_3O_4 nanohybrid will benefit immobilization of probes and subsequent sensing.

Optimization of biotin-$cDNA_{OTA}$-Au/Fe_3O_4 NP-based OTA aptasensor

Scheme 1 shows that binding of the OTA aptamer with its corresponding cDNA inhibits biotin–SA-ALP bonding thus leading

Fig. 3 Composition of Au/Fe_3O_4 nanohybrid. (A) XPS survey of Fe_3O_4 NP and Au/Fe_3O_4 nanohybrid; (B) high-resolution XPS spectra of Au 4f of Au/Fe_3O_4 nanohybrid; (C) XRD spectra of Fe_3O_4 NP and Au/Fe_3O_4 nanohybrid.
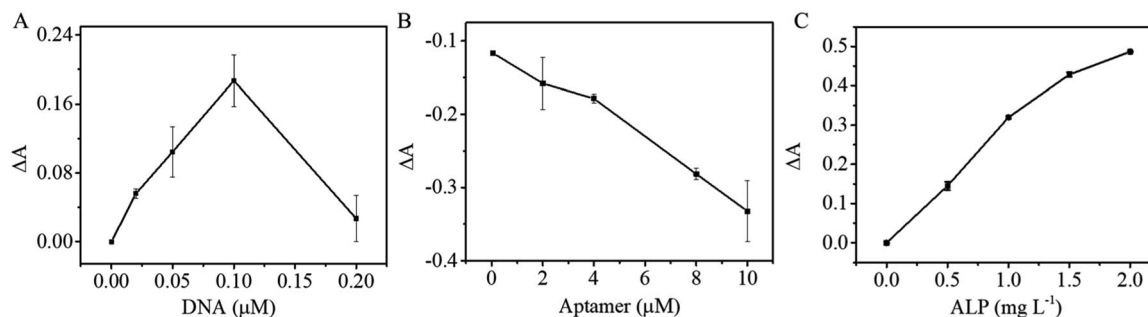
Fig. 5 Optimization experimental conditions of OTA detection: (A) concentration of DNA; (B) concentration of APT; (C) concentration of SA-ALP.

to less *p*-NPP hydrolysis. To achieve sound sensing performance, the amount of cDNA probes on Au/Fe$_3$O$_4$ nanohybrid, OTA aptamers, and SA-ALP were optimized. Different concentrations of biotin-cDNA-SH were applied to prepare biotin-cDNA-Au/Fe$_3$O$_4$ nanohybrid. Then, SA-ALP was added. The pellet obtained *via* magnetic separation was re-dispersed in *p*-NPP solution. The stronger yellow color indicates that a larger amount of biotin-cDNA is successfully immobilized on Au/Fe$_3$O$_4$ nanohybrid for OTA sensing. First, the amount of biotin-cDNA used in the reaction system was optimized. Fig. 5A shows that the relative UV-visible absorbance intensity (Δ*A*) increases with the concentration of biotin-cDNA and then reaches its maximum at a biotin-cDNA concentration of 0.1 μM. Additional biotin-cDNA does not enhance the signal further. In contrast, when the DNA concentration is higher than 0.1 μM, the absorbance at 405 nm decreases again probably due to the steric hindrance. Hence, the optimal concentration of biotin-cDNA-SH was selected to be 0.1 μM.

The OTA competes for binding to the OTA aptamer and its cDNA; thus, the amount of OTA aptamer applied to the sensing system was optimized next. When the concentration of biotin-cDNA used in the reaction is 0.1 μM, the relative absorbance Δ*A* decreases with OTA aptamer concentration increases, indicating that the aptamer pairs with the complementary DNA. Thus, this complex covers the biotin molecule at the end of the DNA and inhibits binding between biotin and SA-ALP (Fig. 5B).

A concentration of 10 μM aptamer was selected from a reaction efficiency and reagent saving perspective.

The colorimetric signal is largely dependent on the enzymatic reaction of ALP and its substrate; thus, the alkaline phosphatase concentration is also an important parameter for colorimetric biosensors. Then with the optimized cDNA and OTA aptamer concentration, the SA-ALP concentration was titrated. Fig. 5C shows a significant increase in UV-visible absorbance with increasing ALP concentration. A high alkaline phosphatase concentration leads to a higher background; thus, 1.5 mg L^{-1} was used for subsequent reactions.

Analytical performance of biotin-cDNA$_{OTA}$-Au/Fe$_3$O$_4$ NP-based OTA aptasensor

Different concentrations of OTA were introduced into a mixture of OTA aptamer, SA-ALP, and biotin-cDNA-AuNPs/Fe$_3$O$_4$. Fig. 6A shows that the intensity of the absorption at 405 nm increases successively upon incubation with an increasing amount of OTA. A linear relationship was obtained between Δ*A* and the logarithm of the OTA concentrations (inset in Fig. 6A): Δ*A* = 0.064 + 0.13 log(C_{OTA} ng mL^{-1}) (R^2 = 0.95147) from 10 to 100 000 ng mL^{-1}. The detection limit of 1.15 ng mL^{-1} was calculated as 3 times the standard deviation (s.d.) of the blank sample signal (s.d. = 3.13 × 10^{-3}) divided by slope of the regression equation (slope = 0.13). The analytical performance of the proposed OTA aptasensor was compared with the

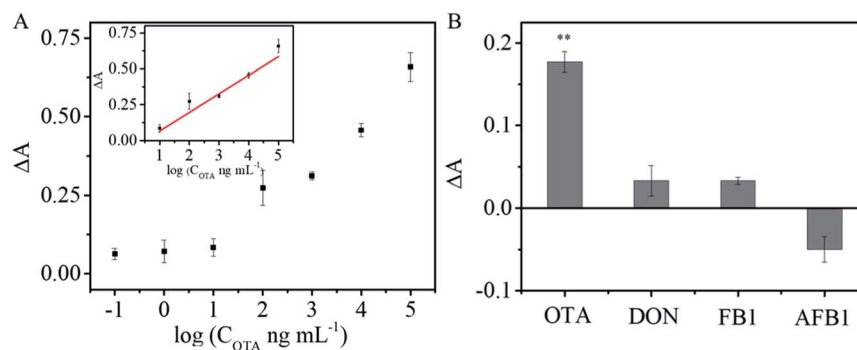**Fig. 6** Analytical performance of the biotin-cDNA$_{OTA}$-Au/Fe$_3$O$_4$ NP-based OTA aptasensor. (A) Signal-dose relationship; inset: the plot of Δ*A* *versus* OTA concentration ranging from 10 to 100 000 ng mL^{-1}. (B) Selectivity of the aptasensor over OTA (10 μg mL^{-1}) and against other mycotoxins. PBS was used as the blank control, ** indicates $p < 0.01$.

Table 1 Comparison of analytical performance of different methods for OTA determination

Nanomaterials	Separation method	Linear range	Limit of detection	Reference
G-rich DNA	—	1.1–4.03 ng mL^{-1}	1.1 ng mL^{-1}	36
Au NPs	—	8.06–251.88 ng mL^{-1}	8.06 ng mL^{-1}	37
Au NPs	Centrifugal separation	—	0.02 ng mL^{-1}	28
Hairpin DNA	—	0.004–0.128 ng mL^{-1}	0.004 ng mL^{-1}	1
G-rich DNA	—	1.61–12.11 ng mL^{-1}	1.61 ng mL^{-1}	38
Au/Fe$_3$O$_4$	Magnetic separation	10–100 000 ng mL^{-1}	1.15 ng mL^{-1}	This work

Table 2 Detection of trace amount of OTA in real sample

Sample	Spiked OTA (ng mL^{-1})	This method			Commercial ELISA		
		Detected (ng mL^{-1})	Recovery (%)	CV (%)	Detected (ng mL^{-1})	Recovery (%)	CV (%)
Peanuts	5	5.205 ± 0.331	104.1%	6.36%	5.054 ± 1.239	101.1%	24.51%
	10	10.791 ± 0.351	107.9%	3.25%	10.269 ± 1.715	102.7%	16.71%
	20	21.081 ± 1.357	105.4%	6.44%	18.837 ± 4.017	94.2%	21.33%
Corns	5	5.019 ± 0.376	100.4%	7.50%	4.796 ± 0.454	95.9%	9.47%
	10	11.208 ± 0.839	112.1%	7.48%	10.075 ± 0.459	100.8%	4.56%
	20	19.755 ± 1.479	98.6%	7.49%	20.633 ± 1.477	103.2%	7.16%
Wine	5	5.520 ± 0.361	110.4%	6.53%	7.159 ± 1.912	143.2%	26.71%
	10	10.252 ± 0.640	102.5%	6.24%	9.230 ± 0.735	92.3%	7.97%
	20	19.100 ± 2.007	95.5%	10.51%	15.700 ± 2.722	78.25%	17.66%

previously reported colorimetric aptasensors (Table 1). This LOD is comparable with or better than those obtained using other nanomaterial-based sensors for OTA.

Specificity is of great importance for practical applications of sensors. To evaluate the specificity of the developed aptasensor, interferences from three other common mycotoxins (AFB1, FB1, and DON) were tested under identical conditions. Negligible responses were observed from FB1, AFB1, and DON, but strong OTA signal was obvious (Fig. 6B; $p < 0.01$). The results demonstrate that the colorimetric aptasensor has good specificity for OTA detection due to the high binding affinity and specificity between OTA and its aptamer.

To verify applicability and accuracy, trace amounts of OTA were spiked into peanut, corn extracts and wine, and measured *via* the proposed colorimetric aptasensor. Table 2 shows that the recovery rates of the peanut, corn and wine samples range from 104.1% to 107.9% with coefficient of variation (CV) of 3.25–6.44%, 98.6–111.2% with the CV of 7.48–7.50%, 95.5–110.14% with the CV of 6.24–10.51%, respectively. At the same time, the samples were further tested by using commercial ELISA kit. The corresponding recovery rates are 94.2–101.1% with CV of 16.71–24.51% for peanut extracts, 95.9–103.2% with CV of 4.56–9.47% for corn extracts, respectively. However, the analytical performance with wine sample is not as good as those in testing peanut and corn extracts. The recovery rates of wine sample range from 78.5%–143.2% with the CV of 7.97–17.66%. The comparatively poor performance in testing wine sample may be caused by the polyphenolic compounds in wine, which potentially disturb signal readings. Successful detecting trace amount of OTA in peanut, corn and wine samples further demonstrated the potential of proposed aptasensor in real sample analysing.

Conclusions

A biotin-cDNA$_{OTA}$-Au/Fe$_3$O$_4$ nanohybrid-based OTA aptasensor was prepared for the colorimetric detection of OTA. The Au/Fe$_3$O$_4$ nanohybrid offered magnetic separation and immobilized biotin-cDNA as a probe for OTA detection. Under optimized conditions, the linear working range was 10 ng mL^{-1} to 100 μg mL^{-1}, and the LOD was 1.15 ng mL^{-1}. Trace amounts of OTA were easily detected in peanut and corn extracts confirming the potential of this technique for real sample analysis.

Conflicts of interest

There are no conflicts to declare.

Acknowledgements

Notes and references

1 C. Wang, X. Dong, Q. Liu and K. Wang, *Anal. Chim. Acta*, 2015, **860**, 83–88.

2 A. el Khoury and A. Atoui, *Toxins*, 2010, **2**, 461–493.

3 A. Hayat, C. Yang, A. Rhouati and J. L. Marty, *Sensors*, 2013, **13**, 15187–15208.

4 A. Pfohl-Leszkowicz and R. A. Manderville, *Mol. Nutr. Food Res.*, 2007, **51**, 61–99.

5 H. Badie Bostan, N. M. Danesh, G. Karimi, M. Ramezani, S. A. Mousavi Shaegh, K. Youssefi, F. Charbgoo, K. Abnous and S. M. Taghdisi, *Biosens. Bioelectron.*, 2017, **98**, 168–179.

6 R. K. Mishra, A. Hayat, G. Catanante, G. Istamboulie and J. L. Marty, *Food Chem.*, 2016, **192**, 799–804.

7 S. M. Sanzani, M. Reverberi, C. Fanelli and A. Ippolito, *Toxins*, 2015, **7**, 812–820.

8 M. Blank and M. Blind, *Curr. Opin. Chem. Biol.*, 2005, **9**, 336–342.

9 L. Pussemier, J. Y. Piérard, M. Anselme, E. K. Tangni, J. C. Motte and Y. Larondelle, *Food Addit. Contam.*, 2006, **23**, 1208–1218.

10 X. Zhao, Y. Yuan, X. Zhang and T. Yue, *Food Control*, 2014, **46**, 332–337.

11 L. C. Huang, N. Zheng, B. Q. Zheng, F. Wen, J. B. Cheng, R. W. Han, X. M. Xu, S. L. Li and J. Q. Wang, *Food Chem.*, 2014, **146**, 242–249.

12 I. Bazin, E. Nabais and M. Lopez-Ferber, *Toxins*, 2010, **2**, 2230–2241.

13 A. Roland, P. Bros, A. Bouisseau, F. Cavelier and R. Schneider, *Anal. Chim. Acta*, 2014, **818**, 39–45.

14 L. Yang, Y. Zhang, R. Li, C. Lin, L. Guo, B. Qiu, Z. Lin and G. Chen, *Biosens. Bioelectron.*, 2015, **70**, 268–274.

15 S. Wu, N. Duan, X. Ma, Y. Xia, H. Wang, Z. Wang and Q. Zhang, *Anal. Chem.*, 2012, **84**, 6263–6270.

16 J. Qian, X. Yang, Z. Yang, G. Zhu, H. Mao and K. Wang, *J. Mater. Chem. B*, 2015, **3**, 1624–1632.

17 Y. Song, W. Wei and X. Qu, *Adv. Mater.*, 2011, **23**, 4215–4236.

18 M. Liu, Z. Wang, T. Tan, Z. Chen, X. Mou, X. Yu, Y. Deng, G. Lu and N. He, *Theranostics*, 2018, **8**, 5772–5783.

19 R. Huang, L. He, Y. Xia, H. Xu, C. Liu, H. Xie, S. Wang, L. Peng, Y. Liu, Y. Liu, N. He and Z. Li, *Small*, 2019, **15**, e1900735.

20 M. Wang, D. Yue, Q. Qiao, L. Miao, H. Zhao and Z. Xu, *Chin. Chem. Lett.*, 2018, **29**, 703–706.

21 M. Liu, A. Khan, Z. Wang, Y. Liu, G. Yang, Y. Deng and N. He, *Biosens. Bioelectron.*, 2019, **130**, 174–184.

22 Y. Liu, Y. Deng, T. Li, Z. Chen, H. Chen, S. Li and H. Liu, *J. Biomed. Nanotechnol.*, 2018, **14**, 2156–2161.

23 Q. Yuan, D. Lu, X. Zhang, Z. Chen and W. Tan, *TrAC, Trends Anal. Chem.*, 2012, **39**, 72–86.

24 S. Jiang, K. Y. Win, S. Liu, C. P. Teng, Y. Zheng and M.-Y. Han, *Nanoscale*, 2013, **5**, 3127.

25 J. Yan, L. Wang, L. Tang, L. Lin, Y. Liu and J. Li, *Biosens. Bioelectron.*, 2015, **70**, 404–410.

26 M. Gu, J. Liu, D. Li, M. Wang, K. Chi, X. Zhang, Y. Deng, Y. Ma, R. Hu and Y. Yang, *Nanosci. Nanotechnol. Lett.*, 2019, **11**, 1139–1144.

27 Z. Wang and L. Ma, *Coord. Chem. Rev.*, 2009, **253**, 1607–1618.

28 R. Xiao, D. Wang, Z. Lin, B. Qiu, M. Liu, L. Guo and G. Chen, *Anal. Methods*, 2015, **7**, 842–845.

29 Y. Wei, J. Zhang, X. Wang and Y. Duan, *Biosens. Bioelectron.*, 2015, **65**, 16–22.

30 Z. Xi, B. Zheng and C. Wang, *Nanosci. Nanotechnol. Lett.*, 2016, **8**, 1061–1066.

31 C. Wang, J. Qian, K. Wang, X. Yang, Q. Liu, N. Hao, C. Wang, X. Dong and X. Huang, *Biosens. Bioelectron.*, 2016, **77**, 1183–1191.

32 Y. Liu, J. Yu, Y. Wang, Z. Liu and Z. Lu, *Sens. Actuators, B*, 2016, **222**, 797–803.

33 Y. Xing, Y. Jin, J. Si, M. Peng, X. Wang, C. Chen and Y. Cui, *J. Magn. Magn. Mater.*, 2015, **380**, 150–156.

34 X. Ren, P. Lu, R. Feng, T. Zhang, Y. Zhang, D. Wu and Q. Wei, *Talanta*, 2018, **188**, 593–599.

35 T. Zeng, X. Zhang, Y. Ma, H. Niu and Y. Cai, *J. Mater. Chem.*, 2012, **22**, 18658.

36 C. Yang, V. Lates, B. Prieto-Simon, J. L. Marty and X. Yang, *Biosens. Bioelectron.*, 2012, **32**, 208–212.

37 C. Yang, Y. Wang, J. L. Marty and X. Yang, *Biosens. Bioelectron.*, 2011, **26**, 2724–2727.

38 C. Yang, V. Lates, B. Prieto-Simon, J. L. Marty and X. Yang, *Talanta*, 2013, **116**, 520–526.